ISSN 0029-3865

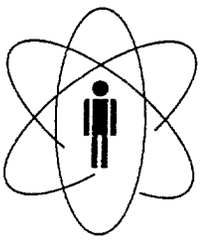

CBPF - CENTRO BRASILEIRO DE PESQUISAS FÍSICAS
Rio de Janeiro

Notas de Física

CBPF-NF-038/96
July 1996

Fission of ^{209}Bi by 60-270 MeV Tagged Photons: Cross Section Measurement and Analysis of Photofissility

M.L. Terranova, G.Ya. Kezerashvili, V.A. Kiselev, A.M. Milov, S.I. Mishnev, I.Ya. Protopopov, V.N. Rotaev, D.N. Shatilov and O.A.P. Tavares

CNPq - Conselho Nacional de Desenvolvimento Científico e Tecnológico

FISSION OF ^{209}Bi BY 60-270 MeV TAGGED PHOTONS: CROSS SECTION MEASUREMENT AND ANALYSIS OF PHOTOFISSILITY

M.L.Terranova
Dipartimento di Scienze e Tecnologie Chimiche, Universita' di Roma "Tor Vergata", Via della Ricerca Scientifica, 00133 Roma , Italy and
Istituto Nazionale di Fisica Nucleare, Sezione di Roma 2, Roma, Italy

G.Ya.Kezerashvili, V.A.Kiselev, A.M.Milov, S.I.Mishnev, I.Ya.Protopopov, V.N.Rotaev, and D.N.Shatilov
Budker Institute of Nuclear Physics, Academician Lavrentyev, 11 , 630090 Novosibirsk, Russia

O.A.P.Tavares
Conselho Nacional de Desenvolvimento Cientifico e Tecnologico-CNPq, Centro Brasileiro de Pesquisas Fisicas-CBPF, 22290-180 Rio de Janeiro-RJ, Brazil

ABSTRACT

Tagged photons produced by the ROKK-2 facility have been used to measure the photofission cross section of ^{209}Bi in the energy range 60-270 MeV .
Photofission events were detected by using a nuclear fragment detector designed for fission experiments, based on multiwire spark counters.
Fissility values have been deduced and compared with available data obtained in other laboratories by using monochromatic photons. These data, together with early measurements obtained near photofission threshold, have been analysed in the framework of a two-step model which considers the primary photointeraction occurring *via* the quasi-deuteron and/or photomesonic processes, followed by a mechanism of evaporation-fission competition for the excited residual nucleus.
The model was found to reproduce the main experimental features of ^{209}Bi photofissility up to 300 MeV.

PACS numbers: 25.20.-x , 24.10.-i , 25.85.Jg

Key-words: Photonuclear reactions; Photofission; Photofissility.

I. INTRODUCTION

The study of fission phenomenon induced in pre-actinide nuclei by electromagnetic probes yields fundamental information on the nuclear photoexcitation mechanisms. In view of the relatively high value of the fission barrier height of such nuclei (~ 20-30 MeV), the photofission cross sections depend strongly upon the excitation energy left in the nucleus after emission of the fast products . The analysis of fission reactions may thus give complementary information to that achieved from the study of light-particle emission processes.

The photofission of ^{209}Bi has been investigated since the early fifties, when Bernardini et al . [1] for the first time pointed out a rapid increase of the fission cross section with increasing incident photon energy in the range 125-305 MeV. After that, many experimental determinations of ^{209}Bi photofission cross section were performed by using bremsstrahlung beams in the energy range from near the fission threshold (~ 23 MeV) [2] up to 16 GeV [3].

In recent years, the possibility of using monochromatic (or quasi-monochromatic) photon beams allowed researchers to obtain more reliable photofission data at intermediate energies ($k \leq 0.3$ GeV) [4-8] . Here we present recent results obtained by using the ROKK-2 facility at the storage ring VEPP-3 (BINP, Novosibirsk, Russia). The ^{209}Bi photofission cross section has been measured with monochromatic tagged photons in the energy range 60-270 MeV, taking advantage of a fission fragment detector (FF) designed for fission experiments at intermediate energies [9].

Along with the experimental cross sections, the present paper reports a detailed analysis of the resulting fissility data , and a comparison with those evaluated in the framework of a simple two-step photointeraction model for intermediate- energy fission reactions . According to this model, in the first stage of the reaction, the absorption of the incoming photon is assumed to occur by a neutron-proton pair (quasi-deuteron mechanism, QD) or , at energies higher than 140 MeV, by individual bound nucleons (photomesonic mechanism ,PM). The primary interaction is followed by de-excitation of the residual nucleus through a mechanism of competition between particle evaporation and fission .

In order to calculate nuclear fissility for photon energies $k \leq 140$ MeV, use has been made of the nuclear transparency to neutron and proton in their final states. The nuclear transparency, τ , is the chief quantity which gives the percentage of

formation of the residual nucleus. For k ≥ 140 MeV the average characteristics of the residual nuclei after photoabsorption have been taken from Monte Carlo calculations on photon-induced intranuclear cascade [10] .Finally, the quantity r = a_f / a_n (ratio of the level density parameter at the fission saddle point to that after neutron evaporation) has been treated as an adjustable parameter, to be determined semi-empirically .

II. EXPERIMENTAL PROCEDURE

A schematic view and main parameters of the backscattered laser photon facility ROKK-2 at the storage ring VEPP-3 (Novosibirsk, Russia) are presented in Fig.1. Compton and bremsstrahlung gamma quanta left the straight section through the 0.1 radiation length mirror (M5), passing successively through vacuum tube, cleaning magnet , plastic scintillator counters , fission fragment detector and γ-beam monitoring system. A detailed description of the ROKK-2 facility may be found in Refs. [11] and [12] .

The γ-beam profile (about 3 cm in diameter) was measured by two multiwire proportional chambers (MWPC) with a thin lead convertor, and the energy by the total photoabsorption γ-spectrometer (NaI(Tl) 11x11x44 cm) or by a Pb-plastic scintillator sandwich counter (SW). The first one was used mainly for calibration, the second one for dose measurements. The energy resolution at k =140 MeV was 6% and 13% for NaI(Tl) and SW, respectively.

The tagging system [13,14] placed beside the bending magnet BM2 operated on the basis of two drift chambers ,each one having seven drift gaps. The tagging system could analyse the momentum of the scattered electrons corresponding to gamma-quanta of 30-270 MeV at 2 GeV electron beam energy , with energy resolution of 4 MeV and efficiency 100% . In view of the low counting rate expected for Bi fission, the energy bin width of the tagging system was increased up to 30 MeV.

For the present experiment use has been made of a nuclear fission fragment detector (FF) based on multiwire spark counters (SC). A total of 21 counters were placed inside the FF vessel (diameter 35 cm , length 80 cm) filled with a 98.7% He +1.3% Ne mixture at 1 atm . Details of the detecting apparatus have

already been published [9].

The targets (4cm in diameter) were located inside the FF vessel at a distance of 3 mm from the spark counter anodes. The bismuth targets consisted of high-purity metal films prepared by vacuum evaporation on aluminium plates 30-μm thick. We used a stack of nine thick (20 - 60 mg/cm^2) and three thin (1.36 ± 0.05 mg/cm^2) bismuth layers.

By employing the thicker targets a good counting statistics could be achieved. The data stored for the thinner targets were used to estimate the effective target thickness for fission fragment emission from the thicker targets. From the measurements of the current experiment the effective thickness of these last targets was found to be (4.7 ±0.5) μm. If one considers the SC registration threshold of 5 .4 MeV, this value is consistent with that of 6.1 μm evaluated following the procedure described in Ref. [15].

Along with the bismuth targets ,we exposed also three targets of ^{238}U (1 mg/cm^2) , and five uncoated aluminium plates. Information obtained from the uranium targets were used to control data treatment, on the basis of the absolute fission cross section of ^{238}U previously measured at the ROKK-2 facility [16]. The data from aluminium plates allowed us to evaluate the contribution arising from ^{27}Al fission.

One more stack with ^{252}Cf was used to control the registration efficiency of the spark counters, which was (21.0 ± 0.8) % .

The procedure adopted for data acquisition, calibration methodology, background and random coincidence measurements was similar to that published in Refs. [16] and [17] .

III. RESULTS AND COMPARISON WITH OTHER DATA

A. Photofission cross section

The values of the photofission cross section ,σ_f , measured in the present experiment for ^{209}Bi target nucleus are reported in Fig.2 (filled circles). The error bars represent statistical plus systematic uncertainties. Data from other laboratories have been also reported. The data show a systematic increase of

the cross section with increasing photon energy k, although discrepancies among the σ_f - values become large at $k \gtrsim 200$ MeV. Good agreement is found with the results obtained by using monochromatic photons [5,6] and also with the σ_f - curve obtained by the technique of virtual photons by Arruda-Neto et al.[21] . For $k \gtrsim 230$ MeV, however, these latter cross sections show a more pronounced increase with energy .

The value of the fission threshold energy for ^{209}Bi , i.e., the ground-state fission barrier height B_{f_0}, has been determined from a least-squares analysis of the fission cross sections measured at $k \leq 50$ MeV [2, 4, 20] by using an expression of the type $\sigma_f = c\,(k - B_{f_0})^4$. The fitting procedure gives $B_{f_0} = (22.0 \pm 1.1)$ MeV , a value which is found to compare rather well with the fission barrier height already obtained by using different procedures [2,23-27] and reported in Table I. An average value $B_{f_0} = (22.5 \pm 1.3)$ MeV has been deduced from these data.

B. Nuclear photofissility

The nuclear fissility, f , represents the total fission reaction probability after absorption of the incoming photon by the target nucleus, and is given by the ratio of the fission cross section ,$\sigma_f(k)$, to the total nuclear photoabsorption cross section, $\sigma_a^T(k)$, i.e.,

$$f(k) = \frac{\sigma_f(k)}{\sigma_a^T(k)} \quad . \tag{1}$$

In order to deduce the fissility-values of ^{209}Bi it is necessary to obtain the $\sigma_a^T(k)$-values in the energy range from near fission threshold up to 300 MeV. In the energy range 30-140 MeV the total photoabsorption cross section has been calculated in the framework of Levinger's modified quasi-deuteron model [28] by the expression :

$$\sigma_a^T = L\frac{NZ}{A}\sigma_{\gamma d}^f(k)e^{-D/k} \quad , \tag{2}$$

where $\sigma^f_{\gamma d}(k)$ is the total photodisintegration cross section of the free deuteron, NZ is the number of neutron-proton pairs in the nucleus, and L and D are, respectively, the so called "Levinger's" and "damping" parameters, both depending on the mass number A : $L = 6.8 - 11.2\ A^{-2/3} + 5.7\ A^{-4/3}$ [29], and $D = 0.72\ A^{0.81}$ MeV [30]. As far as $\sigma^f_{\gamma d}(k)$ is concerned, values have been taken from the compilation of Rossi et al. [31].

For energies above the pion photoproduction threshold, the total nuclear photoabsorption cross section has been evaluated by summing the contributions due to both quasi-deuteron and photomesonic mechanisms of primary interaction , i.e.,

$$\sigma^T_a(k) = 83\,\sigma^b_{\gamma p}(k) + 126\,\sigma^b_{\gamma n}(k) + 324\,\sigma^f_{\gamma d}(k) \qquad (3)$$

as explained in details in Ref. [32].

The values of $\sigma^T_a(k)$ obtained for ^{209}Bi as described above are plotted in Fig.3 (full line). Unfortunately, no experimental σ^T_a data are available for Bi. On the basis of the strong dependence of σ^T_a upon the mass number, we decided ,for the sake of comparison, to report in Fig.3 the total nuclear photoabsorption cross sections measured for Pb in the energy range $30<k\leq 132$ MeV [33] and $145\leq k\leq 300$ MeV [34, 35]. As one can appreciate , the calculated trend results in substantial agreement with both the low- and high-energy σ^T_a - data , and it can therefore be used in evaluating the ^{209}Bi photofissility up to 300 MeV.

The fissility values deduced from the photofission cross sections measured in the present experiment are presented in Fig.4 (filled circles) along with literature data obtained by using monochromatic photon beams [4-8]. Also reported in Fig.4 are the data by Warnock and Jensen [2] (open triangles), for they represent the unique set of measurements taken near the photofission threshold. From the inspection of Fig.4 it is seen that fissility increases by six order of magnitude with incident photon energy from 25 MeV up to 180 MeV , whereas a slight decrease is detected at the higher energies. A theoretical interpretation of the data reported in Fig.4, also including the evaluation of fissility values, will be developed in the next section.

IV. DATA ANALYSIS AND DISCUSSION

A. A two-step model for photofission reactions

The nuclear fissility for the target nucleus ^{209}Bi has been evaluated within the framework of the currently accepted, two-step model for intermediate-energy photofission reactions. In the first step the absorption of the incoming photon is assumed to occur by the interaction with correlated neutron-proton pairs (quasi-deuteron absorption, QD) or with individual bound nucleons (photomesonic interaction, PM). The recoil nucleons and/or photoproduced pions generate a rapid intranuclear cascade which yields, at the end of the process, a residual nucleus with a certain excitation energy. In a second stage, after termodynamic equilibrium has been reached, the residual nucleus de-excites through a mechanism of competition between fission and particle evaporation. Accordingly, fissility can be evaluated by multiplying the average probability of formation of the residual nucleus by the total fission probability for such residual. The model has successfully explained the main features of fissility at intermediate energies for actinide as well as for pre-actinide target nuclei [8, 10,16,36-42]. One must keep in mind, however, that fissility calculated within the framework of the above model has been found strongly dependent on the values of some nuclear parameters involved in the calculation, such as the level density parameter and the height of fission barrier.

Details about the calculation procedure adopted in the present work will be presented below.

B. Nuclear photoabsorption mechanisms

For photon energies up to 140 MeV, the nuclear photoabsorption is described in terms of the interaction between the incoming photon and a quasi-deuteron as proposed by Levinger [43] and recently detailed by Tavares and Terranova [41]. The nucleus is considered as a degenerate Fermi gas of non-interacting neutrons and protons confined within a spherically symmetric nuclear potential. Relativistic kinematics and the Pauli exclusion principle are applied to the interaction $\gamma + (n\text{-}p) \rightarrow n^* + p^*$ in order to determine the kinetic energies of neutron (T_{n^*}) and proton (T_{p^*}) in their final states inside the nucleus , thus obtaining [41]

$$T_{n^*} = a\,(1 - b\cos\Theta') - m \;; \qquad T_{p^*} = a\,(1 + b\cos\Theta') - m \;. \tag{4}$$

Here, m is the nucleon rest mass, Θ' is the proton polar-angle in the center-of mass-system, $a = m + k/2 + 3\,(E_F^n + E_F^p)/10$,and b is a constant which depends on photon energy ,k , and on the Fermi energy for neutron (E_F^n) and proton (E_F^p) . For ^{209}Bi , $E_F^n = 37.8$ MeV and $E_F^p = 28.6$ MeV.
Due to the restrictions imposed by the Pauli exclusion principle, the lower values for T_{n^*} and T_{p^*} are E_F^n and E_F^p , respectively. From Eqs. (4) it follows

$$E_F^n \le a\,(1 - b\cos\Theta') - m \qquad \text{and} \qquad E_F^p \le a\,(1 + b\cos\Theta') - m \;. \tag{5}$$

By summing up these inequalities , the photon energy threshold for the QD absorption in ^{209}Bi is determined as $k_{th}(Q.D) \approx 27$ MeV.

Following the formalism developed in Ref. [41], retention of both neutron and proton after the primary photointeraction results whenever the restrictions $T_{n^*} \le E_C^n$ and $T_{p^*} \le E_C^p$ are simultaneously satisfied. Here, the E_C's represent the cut-off energy, defined as the Fermi energy plus the binding energy of the loosest nucleon plus, in the case of proton, the Coulomb energy at the nuclear surface . For ^{209}Bi we have $E_C^n = 45.3$ MeV and $E_C^p = 46.8$ MeV for neutron and proton, respectively. By using Eqs.(4) and the limiting conditions above, it follows that neutron and proton remain simultaneously retained within the Bi target for incident energies not exceeding ~ 52 MeV. As a result, in the energy range $27 \le k \le 52$ MeV, the residual nucleus formed after the primary QD photointeraction is ^{209}Bi with excitation energy $E^* = k$.

In the energy range $52 \le k \le 140$ MeV an average probability $\overline{p} < 1$ still exists that both the neutron and the proton remain absorbed within the target nucleus.

The other three possible modes of formation of the residual nucleus , i) proton escaping with neutron retention, ii) neutron escaping with proton retention ,iii) simultaneous escaping of both nucleons from the nucleus, do not contribute to fission , in view of the low value of both formation probability and average excitation energy for these residuals .

The probability for a nucleon to escape from the nucleus without suffering any

secondary interaction is given by the nuclear transparency to neutron (τ_n) and proton (τ_p) . Following the scheme proposed in Ref.[41], the average probability of simultaneous absorption of neutron and proton , $\overline{p}$, can be calculated as a function of k through the expression

$$\overline{p} = 1 - \overline{p}_0 - \overline{p}_1 - \overline{p}_2 \quad , \tag{6}$$

where

$$\overline{p}_0 \approx \frac{\alpha'+\beta'\varepsilon}{d}\left\{\alpha(\varepsilon - E_C^p - E_C^n) + \beta\left[(\varepsilon - E_C^p)^2 - E_C^{n^2}\right]\right\} + \frac{\beta'\gamma}{d}\left\{\frac{\varepsilon}{3}\left[\frac{1}{E_C^{n^3}} - \frac{1}{(\varepsilon - E_C^p)^3}\right] - \frac{1}{2}\left[\frac{1}{E_C^{n^2}} - \frac{1}{(\varepsilon - E_C^p)^2}\right]\right\} \tag{7}$$

$$\overline{p}_1 = \frac{1}{d}\left\{\alpha(\varepsilon - E_F^p - E_C^n) + \frac{\beta}{2}\left[(\varepsilon - E_F^p)^2 - E_C^{n^2}\right] + \frac{\gamma}{3}\left[\frac{1}{E_C^{n^3}} - \frac{1}{(\varepsilon - E_F^p)^3}\right]\right\} - \overline{p}_0 \tag{8}$$

$$\overline{p}_2 = \frac{1}{d}\left\{\alpha'(\varepsilon - E_C^p - E_F^n) + \frac{\beta'}{2}\left[(\varepsilon - E_F^n)^2 - E_C^{p^2}\right] + \frac{\gamma'}{3}\left[\frac{1}{E_C^{p^3}} - \frac{1}{(\varepsilon - E_F^n)^3}\right]\right\} - \overline{p}_0 \quad . \tag{9}$$

The quantities ε and d are expressed as

$$\varepsilon = k + \tfrac{3}{5}(E_F^n + E_F^p) \tag{10}$$

$$d = k - \tfrac{2}{5}(E_F^n + E_F^p) \quad . \tag{11}$$

In Eqs.(7-9) α , β, γ and α' , β', γ' are constant (those with prime refer to proton) which define the trend of the nuclear transparencies to emerging nucleons, according to the general formula

$$\tau_i = \alpha + \beta T_i + \frac{\gamma}{T_i^4} \qquad , \quad i = n^* , p^* . \tag{12}$$

For neutron ($i = n^*$) we get

$$\alpha = \tau_i^{min} - \frac{5\gamma}{T_i^{min^4}} \tag{13}$$

$$\beta = \frac{4\gamma}{T_i^{min^5}} \tag{14}$$

$$\gamma = \frac{\tau_i^c - \tau_i^{min}}{\frac{4E_c^n}{T_i^{min^5}} + \frac{1}{E_c^{n^4}} - \frac{5}{T_i^{min^4}}} \qquad , \tag{15}$$

and identical expressions are valid for proton, where the changes $n^* \rightarrow p^*$ and $E_C^n \rightarrow E_C^p$ are implicit .

In the above expressions, τ^c stands for the nuclear transparency at the cut-off energy E_C, and τ^{min} for the minimum value of the nuclear transparency at the kinetic energy T^{min}. For ^{209}Bi one obtains :

$$\begin{aligned} E_c^n &= 45.3 MeV \\ E_c^p &= 46.8 MeV \\ T_n^{min} &= 131 MeV \\ T_p^{min} &= 81.3 MeV \end{aligned} \tag{16}$$

and

$$\tau_n^f = 0.807$$
$$\tau_p^f = 0.256$$
$$\tau_n^{min} = 0.208 \qquad (17)$$
$$\tau_p^{min} = 0.110$$

Accordingly, for neutron the constants in Eq.(12) are found to assume the following values:

$$\alpha = 0.163 \quad , \quad \beta = 2.74 \times 10^{-4} \ MeV^{-1} \quad , \quad \gamma = 2.65 \times 10^{6} \ MeV^{4} \quad , \qquad (18)$$

and for proton

$$\alpha' = -3.41 \times 10^{-3} \quad , \quad \beta' = 1.12 \times 10^{-3} \ MeV^{-1} \quad , \quad \gamma' = 0.992 \times 10^{6} \ MeV^{4} \quad . \qquad (19)$$

The average probability $\overline{p}$ of formation of ^{209}Bi nucleus with excitation energy $E^* = k$ has been thus calculated for incident energies ranging between 52 and 140 MeV. The trend of $\overline{p}$ *vs.* k is depicted in Fig. 5a.

In the energy range $140 < k \leq 300$ MeV two different mechanisms contribute to the primary photoabsorption, namely, pion photoproduction (PM) and QD-photodisintegration. At these energies single pion photoproduction *via* baryon resonance states does indeed dominate. The average characteristics of the residual nucleus formed via PM and QD interactions have been deduced from recent Monte Carlo calculations [10] performed within the framework of the intranuclear cascade-model by Barashenkov et al. [36]. The trends of average mass and charge loss obtained in Ref.[10] indicate that the average residual nucleus is ^{208}Pb for incoming photons with $140 \lesssim k \lesssim 230$ MeV, and ^{207}Pb for $230 \lesssim k \lesssim 300$ MeV. The values of the average excitation energy, $\overline{E}^*$, calculated by Guaraldo et al. [10] are reported in Fig.5 b. It is worthnoticing that the $\overline{E}^*$ vs. k curve exhibits a maximum at k=145 MeV and a minimum at k= 180 MeV.

C. De-excitation of the residual nucleus

The main de-excitation channels of a certain average residual nucleus $(\overline{A}^*, \overline{Z}^*, \overline{E}^*)$ formed after either escaping or absorption of the particles partecipating to the primary interaction are fission and neutron emission. For ^{209}Bi target nucleus, however, at excitation energies $E^* \gtrsim 80$ MeV the contribution arising from proton and alpha-particle emission is small, although not negligible. Moreover, the successive chance-emission probabilities for neutron and/or charged particles (p, α) have to be taken into consideration. In all cases, the nuclear fissility can be expressed as:

$$f = \bar{p} P_t \ , \tag{20}$$

where P_t represents the total fission probability of the residual nucleus.
For $E^* \lesssim 80$ Mev, the first- and the second-chance fission probabilities are found to contribute to the total fission probability, whereas for $E^* \gtrsim 80$ MeV higher-order chance-fission probabilities must be considered. These last quantities have been included in the present calculations. On the basis of the considerations presented in the Appendix, we can write as a first approximation

$$P_t \approx 2 f_1 \ , \quad \overline{E}^* \geq 80 MeV \ , \tag{21}$$

with f_1 standing for the first-chance fission probability.
The hyphoteses adopted in the present work in order to evaluate nuclear fissility values for ^{209}Bi are schematically presented in Table II .
The routine calculation used for the evaporation-fission competition is that already developed in Ref.[41] ,and is based on the statistical model proposed by Weisskopf [44] and Vandenbosch and Huizenga [45]. The main lines of the calculation are reported below.
The first-chance fission probability is expressed by:

$$f_1 = \frac{F_1}{1 + F_1 + G_1 + H_1} \ . \tag{22}$$

A similar expression may be written for the second-chance fission probability. The

quantities F, G, and H which represent, respectively, the probability of fission, proton emission and alpha-particle emission,all relative to neutron emission, are written as :

$$F = \frac{15\left[2r^{1/2}a_n^{1/2}(E^* - B_f)^{1/2} - 1\right]}{4rA^{2/3}(E^* - B_n)} \times \exp\left\{2a_n^{1/2}\left[r^{1/2}(E^* - B_f)^{1/2} - (E^* - B_n)^{1/2}\right]\right\} \quad (23)$$

$$G = \frac{E^* - B_p - V_p}{E^* - B_n} \times \exp\left\{2a_n^{1/2}\left[(E^* - B_p - V_p)^{1/2} - (E^* - B_n)^{1/2}\right]\right\} \quad (24)$$

$$H = \frac{2(E^* - B_\alpha - V_\alpha)}{E^* - B_n} \times \exp\left\{2a_n^{1/2}\left[(E^* - B_\alpha - V_\alpha)^{1/2} - (E^* - B_n)^{1/2}\right]\right\} \quad (25)$$

Here,

$$B_f = CB_{f_0} \ , \ V_p = CV_{p_0} \ , \quad V_\alpha = CV_{\alpha_0} \ , \quad (26)$$

where V_{p_0} and V_{α_0} are the Coulomb barriers at the nuclear surface for proton and alpha particle, respectively, and C= 1 - (E*/B) is a correction factor which takes into account for nuclear temperature effects [46]. B_{f_0} is the ground-state fission barrier height, B is the nuclear binding energy, and B_n, B_p and B_α are the separation energies , respectively, for neutron, proton and alpha particle. The values of all quantities used for the various residual nuclei are reported in Ref.[41] .

In order to evaluate the first-chance fission probability f_1 through Eqs.(22-26), we faced the problem of estimating the ratio $r = a_f / a_n$ of the level density parameter at the fission saddle point to that of the residual nucleus after neutron evaporation. In the present calculation we adopted for a_n the expression

$$a_n = \left[a' A + b' A^{2/3} b_s\right]\left\{1+\left[1-e^{-c'(E^*-\Delta)}\right]\times\frac{\Delta M}{(E^*-\Delta)}\right\} MeV^{-1} \qquad (27)$$

recently proposed by Iljinov et al. [47], where $\Delta = 12\ \chi/A^{1/2}$ MeV is the pairing energy (χ=0, 1, or 2, respectively, for odd-odd, odd- even, or even-even nuclei). ΔM is the shell correction in the calculated nuclear mass, and $b_S \approx 1$. The constants $a' = 0.114$, $b' = 0.098$ and $c' = 0.051$ which appear in Eq.(27) are adjustable parameters resulting from the phenomenological systematics of the level densities carried out for several hundred excited nuclides without considering collective effects [47].

The problem of finding reliable values of the ratio $r = a_f / a_n$ represents indeed the critical step in the calculation procedure , in view of the fact that calculated nuclear fissilities turn out to be very sensitive to r-values.

Semi-empirical values of the ratio r for the various residuals have been obtained from the systematics of the 44 experimental fissility data reported in Fig.4. The resulting r-values are shown in Fig.6 as a function of excitation energy, E^*, of the fissioning system. As one can observe, the ratio a_f / a_n decreases with increasing E^* for each residual nucleus. A least-squares treatment of the data yielded the following relationships :

^{209}Bi : $$r = 1+\frac{2.56}{(E^*-22)^{2/3}} \quad , \quad \chi_\nu^2 = 2.5 \qquad (28)$$

^{208}Pb : $$r = 1+\frac{31.88}{(E^*-24)^{6/5}} \quad , \quad \chi_\nu^2 = 3.8 \qquad (29)$$

^{207}Pb : $$r = 1+\frac{31.36}{(E^*-24)^{6/5}} \quad , \quad \chi_\nu^2 = 1.8 \qquad (30)$$

Values of r can therefore be obtained from the above expressions within ~ 1% accuracy.

D. Calculated nuclear fissility and discussion

Nuclear fissilities calculated on the basis of the two-step model for photofission reactions by using the different quantities and parameters discussed in the precedent sub-sections are plotted in Fig.4 (full line). The trend of fissility is found to reproduce rather well (χ^2_ν=2.8) the experimental data of monochromatic photon-induced fission experiments in the entire range of incident energy. The average uncertainty of the calculated fissility values was estimated to be 32%. Inspection of the figure reveals that fissility presents a maximum at k=180 MeV. This feature is better evidenced in the inset graph of Fig.4.

Let us now discuss in some details the most striking features of the present analysis.

Firstly, it is apparent that fissility increases by nearly six order of magnitude as incident photon energy varies from 27 MeV up to ~ 140 MeV. In this energy range, the photoabsorption is described by the interaction of the incoming photon with a neutron-proton pair (QD model). This mechanism leads to a fissioning residual nucleus which , in the favorable case, is the same as the target nucleus with an excitation energy equal to the incident photon energy. Therefore, the fissility behaviour is chiefly governed by the competition between neutron emission and fission . Emission of charged particles is expected also to compete, even if to a lesser extent, at energies $E^* \gtrsim 80$ MeV . Besides, depending on the amount of excitation, fission may take place either as first-chance or higher-order chance during the de-excitation process. In any case, the increase of excitation leads the fission barrier height of residuals to decrease , leading therefore to an enhancement of the fission channel.

Second, it is seen that the trend of fissility shows a broad maximum around k= 180 MeV (see inset in Fig.4). An explanation for this fact may be found by analysing the two-step photofission model developed in the present work. At incident energies in the interval $140 \lesssim k \lesssim 230$ MeV, recoil nucleons and/or photopions resulting from the photomesonic and/or quasi-deuteron photoabsorption mechanisms initiate an intranuclear cascade process . The average compound nucleus formed is ^{208}Pb with maximum excitation energy

of ~ 82 MeV for k ≈ 145 MeV ,and minimum of ~ 75 MeV for k ≈ 180 MeV (Fig.5-b and Ref .[10]). These average characteristics of the residual nucleus, viz. a relatively low excitation energy associated to a fission barrier height larger for the double-magic ^{208}Pb than for its neighbours , are apparently unfavorable in producing an appreciable fission yield. Nevertheless, the evaporation-fission competition works in such a way that for ^{208}Pb the values of the a_f/a_n ratio required in order to reproduce the measured fissility are in the range ~ 1.25 -1.29, this last value being required at k = 180 MeV. These r-values are nearly 7-9% larger than the corresponding ones for Bi in the same range of excitation energy (see Fig.6). In addition, it is supposed that during the de-excitation process the total fission probability of residuals formed at the end of the intranuclear cascade process equals twice the first-chance fission probability (the approximation $P_t \approx 2f_1$). It should be mentioned, moreover, that the trend of fissility deduced from the measured photofission cross sections by Moretto et al. [20] and the curve of total photonuclear absorption cross section of Fig. 3 also exhibit a broad maximum around 180-190 MeV.

Finally, at photon energies approaching 300 MeV, fissility drops by about 30% of its maximum value. At these energies the intranuclear cascade calculations [10] indicate that the average residual formed is ^{207}Pb with excitation energy varying from ~ 83 MeV up to ~ 97 MeV. (Fig.5-b) . At these excitation energies the neutron and/or charged particles evaporation may be enhanced , whereas the a_f/a_n-ratio tends to decrease, leading therefore to a lowering of fissility.

Very recently, Arruda-Neto et al. [48] reported on pion-related effects in the photofission of pre-actinide nuclei. These authors observed for Au and Ta a pronounced dip in the cross section curve near photopion threshold . A pion-related structure around 200-220 MeV was evidenced also in the photofission cross section of ^{209}Bi and ^{208}Pb deduced from the electrofission yields [49] . If one calculates fissility values for ^{209}Bi from the photofission cross section curve of Ref.[21] (full line in Fig.2) and the total absorption cross section curve reported in Fig. 3 , one observes the existence of a maximum at 150 MeV and of a minimum at 210 MeV . These features have not been detected in experiments with monochromatic photons.

As a final remark we wish to point out that, independently of the mechanism of primary photoabsorption, (QD and /or PM) and of the average characteristics

$(\overline{A}^*, \overline{Z}^*, \overline{E}^*)$ of the excited residual nucleus , the r-curves decrease monotonically with increasing E^* (Fig.6). The structureless trend of the r-curves turns out to be unexpected if one observes (Fig.5-b) that, for k>140 MeV, the $\overline{E}^*$ vs. k curve for ^{209}Bi exhibit, on the contrary, a maximum at about 150 MeV and a minimum at about 180 MeV . Overall, the formation of various average residual nuclei (^{209}Bi, ^{208}Pb, and ^{207}Pb) by the photon-induced intranuclear cascade , the consideration of charged particle (p, α) emission competing with fission and neutron emission, and the approximation $P_t \approx 2f_1$ for the occurrence of higher-order chance fission , are found in our view to be the essential physical basis that explains in a satisfactory way the general behaviour of ^{209}Bi photofissility at energies up to 300 MeV .

V. SUMMARY OF THE RESULTS AND CONCLUSIONS

The main results of the present work, which reports the experimental determination of photofission cross section of ^{209}Bi performed with monochromatic tagged photons, are here briefly summarized.

1) The fission of ^{209}Bi induced by tagged photons has been investigated in the range 60-270 Mev by employing a multiwire spark counter for detection of the fission fragments. The cross section data are in good agreement with the ones obtained in other laboratories by using monochromatic photon beams.

2) The cross section data, σ_f, have been normalized to the total nuclear photoabsorption cross section, σ_a^T, obtained by taking into account both quasi-deuteron and photo-mesonic interactions . The deduced fissility values (σ_f / σ_a^T) reveal a rapid increase from near threshold up to 180 MeV, followed by a slight decrease towards 300 MeV.

3) The average value (22.0 $\pm$ 1.1) MeV for the photofission threshold of ^{209}Bi has been deduced from early σ_f -data taken at energies k $\leq$ 50 MeV. This value was found to compare quite satisfactorily with the ground-state fission barrier height of 22.37 MeV obtained from the droplet model by Myers [27].

4) A two step model has been developed in order to obtain calculated values of nuclear fissility . The main assumptions adopted in the calculations are summarized in Table II. The essentials of the model are here recalled: i) for

incident photon energies k < 140 MeV nuclear transparency to neutron and proton in their final states following the QD primary photointeraction has been used to obtain the percentage of formation for the fissioning nucleus (^{209}Bi) ; ii) for k ≥ 140 MeV the average characteristics of the residual nuclei ($\overline{A}^*, \overline{Z}^*, \overline{E}^*$) have been inferred from Monte Carlo calculations of photon-induced intranuclear cascade [10] ; iii) the de-excitation of the average residual nuclei has been described by a mechanism of competition between fission and particle evaporation, where neutron, proton and alpha particle emission modes have been considered throughout ; iv) the higher-order chance fission probabilities have been taken into account through the basic assumption that the total fission probability of a given post-cascade residual equals twice the first-chance fission probability of this residual ($P_t \approx 2\, f_1$) ; v) the ratio a_f/a_n has been treated as an adjustable parameter, the values of which being determined semi-empirically from fissility data reported in Fig.4 . In Fig. 6 it is observed a monotonic trend of a_f/a_n which decreases with increasing excitation energy of the various residuals , indicating asymptotical values (~ 1.03÷1.05) compatible with the phenomenological systematics of level density by Iljinov et al. [47] as well as with the theoretical estimations reported in Refs. [50] and [51] .

5) The ^{209}Bi fissility calculated from the above summarized model is found to reproduce the experimental data rather satisfactorily within the entire range of photon energy (28 - 300 MeV) here investigated (Fig.4). The trend of fissility reveals a not pronounced maximum around 180 MeV.

As a conclusion , we can say that the two-step model for photofission reactions has proved to be rather adequate in interpreting the ^{209}Bi photofissility data reported in the present work. Further studies at energies in the range 140-300 MeV are presently in progress aiming at defining, from both theoretical and experimental point of view, the results here discussed .

VI. APPENDIX : The approximation $P_t \approx 2\, f_1$

Let us consider an excited residual nucleus (Z^*, A^*, E^*) which de-excites via a fission-evaporation competition process . Along with neutron emission, proton and alpha particle emissions may also compete, although to a lesser extent, with the fission mode. This is expected to occur especially when the height of the

fission barrier is comparable with the Coulomb-plus-separation energy of the particle, as for $E^* \gtrsim 80$ MeV. Thus, for the total fission probability we can write formally that

$$\begin{aligned} P_t(Z^*,A^*,E^*) = f_1 &+ n_1 f_{2,n} + p_1 f_{2,p} + \alpha_1 f_{2,\alpha} + n_1 n_{2,n} f_{3,2n} \\ &+ n_1 p_{2,n} f_{3,np} + \cdots\cdots\cdots + p_1 n_{2,p} f_{3,pn} + \cdots\cdots \\ &+ \alpha_1 n_{2,\alpha} f_{3,\alpha n} + \cdots\cdots\cdots, \end{aligned} \tag{31}$$

where the f's, n's, p's and α's represent the values of the probability for, respectively, fissión, neutron emission, proton emission, and alpha particle emission modes. The number in subscripts indicate the chance order of the event. In other words, f_1 is the first-chance fission probability, $f_{3,pn}$ is the third-chance fission probability after successive emission of one proton and one neutron, $\alpha_{2,n}$ is the second-chance probability for alpha particle emission after the first neutron evaporation, and so forth.

The lowest limit for P_t is clearly f_1, because this quantity does not include the contribution of subsequent chance fission probabilities, i.e.,

$$P_t > f_1 \quad . \tag{32}$$

Since generally fissility is given by $f \approx \overline{p} P_t$, where $\overline{p}$ is found in the range 0.4 - 1 for nuclei throughout the Periodic Table (Eq.(6)) , and P_t is expected to retain roughly the trend of the first-chance fission probability of residuals at any step of the evaporation chain ($P_{t_i} \propto f_{1_i}$) , it follows that fissility , f_i , for a given residual i should be of the order of the first-chance fission probability , f_{1_i} .

Results of a number of experiments have shown that fissility of nuclei varies exponentially with both Z^2/A and E^* (Fig.7). Therefore, by considering the first- as well as the successive higher-order-chance fission probabilities, and by noting that the probabilities for the same-order-chance fission are of the same order of magnitude, we can write from Eq. (31) that

$$P_t \approx f_1 + (1 - f_1) f_2 + (1 - f_1)(1 - f_2) f_3 + \cdots\cdots\cdots \quad . \tag{33}$$

An upper limit for P_t is obtained from Eq.(33) as

$$P_t \lesssim 3f_1 - 3f_1^2 + f_1^3 \qquad (34)$$

by considering that the higher-order-chance fission probabilities should be nearly equal to or smaller than the first-chance one ($\cdots \lesssim f_3 \lesssim f_2 \lesssim f_1$), because excitation energy of the new residuals decreases progressively by ~ 10 MeV *per* particle evaporated .

Finally, by taking the average of the two limiting values expressed by Eqs. (32) and (34), and noting that $f_1 < 10^{-1}$ for the nuclei partecipating in the competition process, it follows that the total fission probability can be approximated by

$$P_t \approx 2f_1 \quad . \qquad (35)$$

This approximation has been used throughout the calculations (sub-section IV -c).

ACKNOWLEDGMENTS

The authors wish to express their thanks to Prof. C. Schaerf for useful discussions and suggestions, and to the staff of the VEPR3 storage ring for providing a good quality beam . One of us (O.A.P.T.) wishes to express his gratitude to the Dipartimento di Scienze e Tecnologie Chimiche, Universita' di Roma " Tor Vergata", for the warmest hospitality. The support of the administration of Budker INP (Novosibirsk) and of the Italian INFN (Sezione di Roma 2) is also gratefully acknowledged.

FIGURE CAPTIONS

Fig.1 Experimental lay-out and main parameters of ROKK-2 facility at the VEPP-3 storage ring . BM: bending magnets ; SC: spark counters ; M1-M7 optical mirrors; L1-L3 : focusing lenses ; W1-W3 windows ; TV's: television cameras ; P1-P3 : plastic scintillators ; MWPC : multiwire proportional chambers ; NaI : total photoabsorption γ-spectrometer.

Fig.2 Photofission cross section of ^{209}Bi , σ_f, plotted against incident photon energy, k. Data points are as follows: ◪ , Ref [7] ; ◇, Ref.[8] ; ⊗, Ref.[1]; ○ , Ref.[18]; △, Ref. [19] ; ▲ , Ref. [5]; ■ , Ref. [6] ; □ ,Ref. [20] ; ● present measurements. The full line represents the data of Ref. [21], and the dash-dotted line those of Ref. [22].

Fig.3 Total nuclear photoabsorption cross section for ^{209}Bi, σ_a^T , plotted against photon energy, k. The full line represents the evaluation of σ_a^T according to Eqs.(2) and (3) of the text. Data points are referred to measurements for Pb, and are taken from Ref. [33] (▲), Ref. [34] (○), and Ref.[35] (●).

Fig.4 Nuclear photofissility of ^{209}Bi, f, versus photon energy, k. The points represent the ratio σ_f / σ_a^T of the measured photofission cross section to total nuclear photoabsorption cross section . The σ_a^T values are taken from the curve reported on Fig.3. The experimental σ_f-values are taken from Ref. [2] (▽), Ref. [4] (▼), Ref. [7] (◪), Ref. [8] (◇), Ref. [5] (▲), Ref. [6] (■), and from the present measurements (●). The curve represents the calculated fissility (Sect.IV). The inset graph shows the trend of fissility in the range 100-300 MeV , and the hatched area its uncertainty.

Fig.5 Average probability of formation of ^{209}Bi residual, $\overline{p}$ **(a)** , and average excitation energy, $\overline{E}^*$ **(b)**, plotted against incident photon energy, k, for ^{209}Bi target. The curve shown in **(a)** has been calculated by means of nuclear transparency to neutron and proton (Eqs. (6-19)), and that shown in **(b)** is reproduced from the Monte Carlo intranuclear cascade calculation of Ref. [10].

Fig.6 The ratio $r = a_f/a_n$ plotted against excitation energy for different residuals. The points are r-values semi-empirically determined from the fissility data reported in Fig.4 . The curves are least-squares fitting to data for the various residuals.

Fig.7 Dependence of nuclear fissility on parameter Z^2/A for different values of excitation energy of the fissioning nucleus. The full lines represent the experimental trends taken from Refs. [8,42,52] ; the dashed lines are interpolated trends. The inset graph shows the same dependence, but variables interchanged.

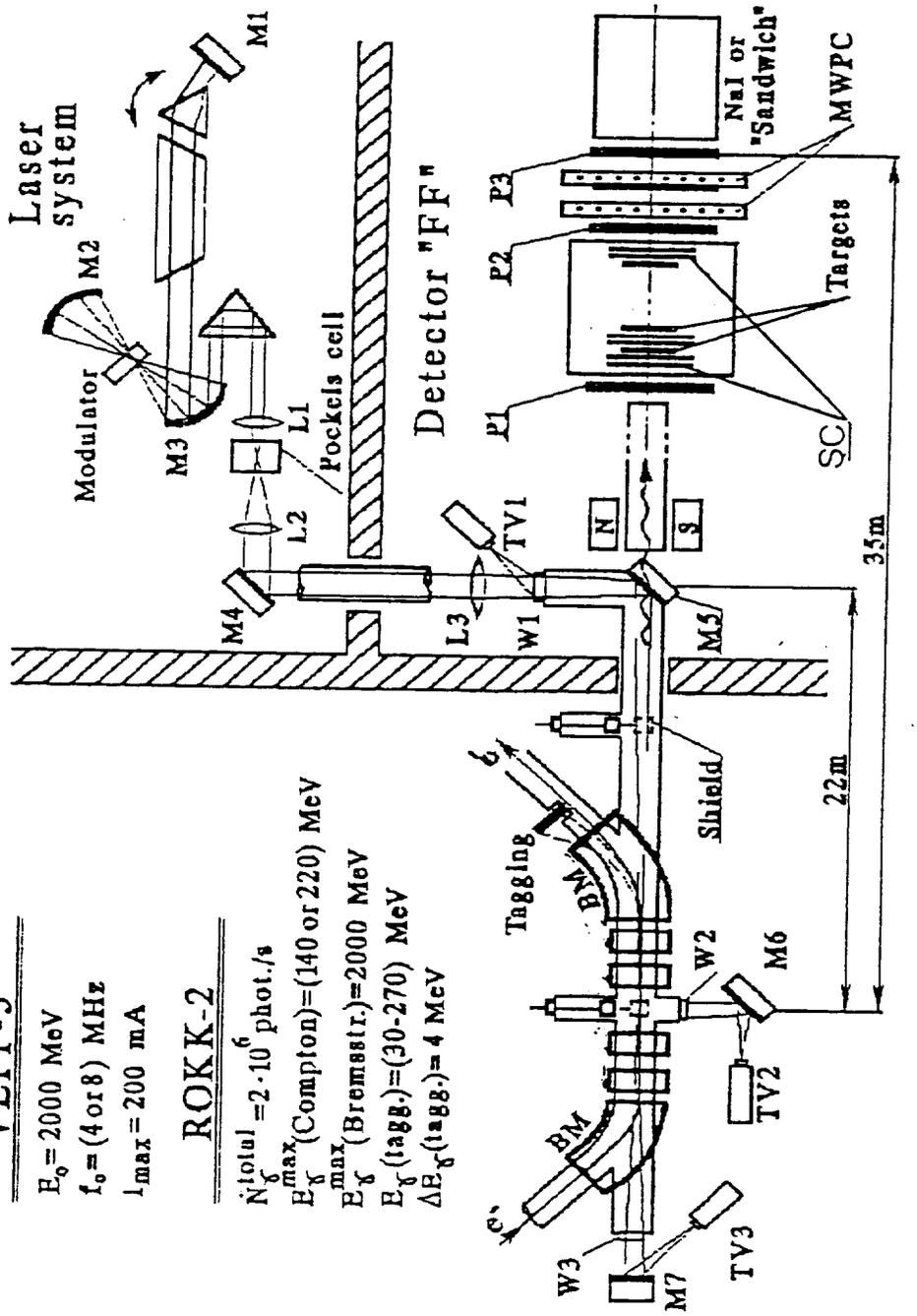
VEPP-3
E_0= 2000 MeV
f_0= (4 or 8) MHz
I_{max}= 200 mA
ROKK-2
$\dot{N}_\gamma^{total}$=2·10^6 phot./s
E_γ^{max}(Compton)=(140 or 220) MeV
E_γ^{max}(Bremsstr.)=2000 MeV
E_γ(tagg.)=(30-270) MeV
ΔE_γ(tagg.)= 4 MeV
Laser system
M1
M2
M3
Modulator
L1
Pockels cell
L2
M4
L3
TV1
W1
Detector "FF"
P1
P2
P3
NaI or "Sandwich"
MWPC
Targets
SC
N
S
35m
M5
Shield
22m
Tagging
BM
W2
M6
TV2
BM
W3
M7
TV3

Fig. 1

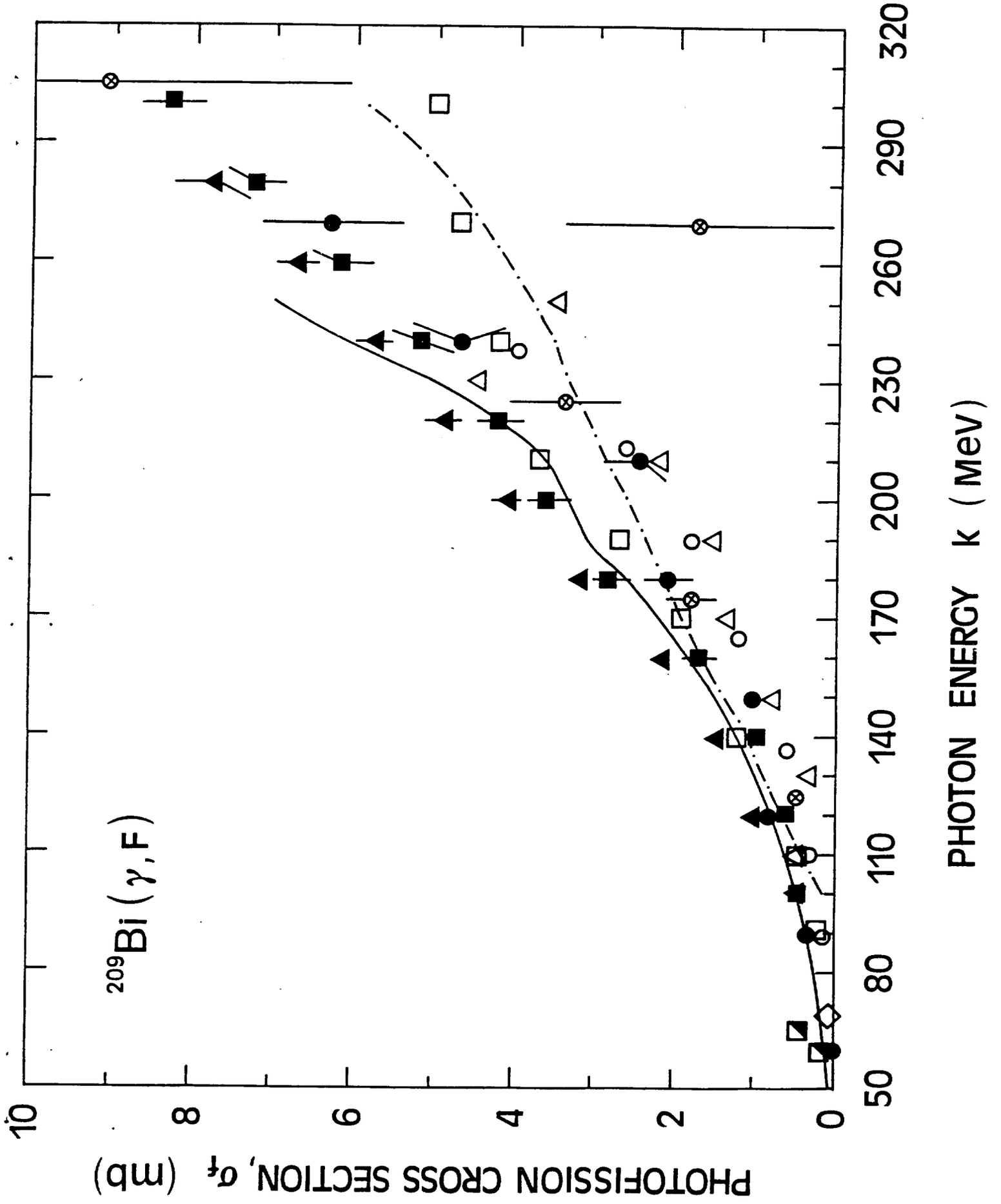
PHOTOFISSION CROSS SECTION, σ_f (mb)
0
2
4
6
8
10
^{209}Bi (γ, F)
50
80
110
140
170
200
230
260
290
320
PHOTON ENERGY k (MeV)

Fig. 2

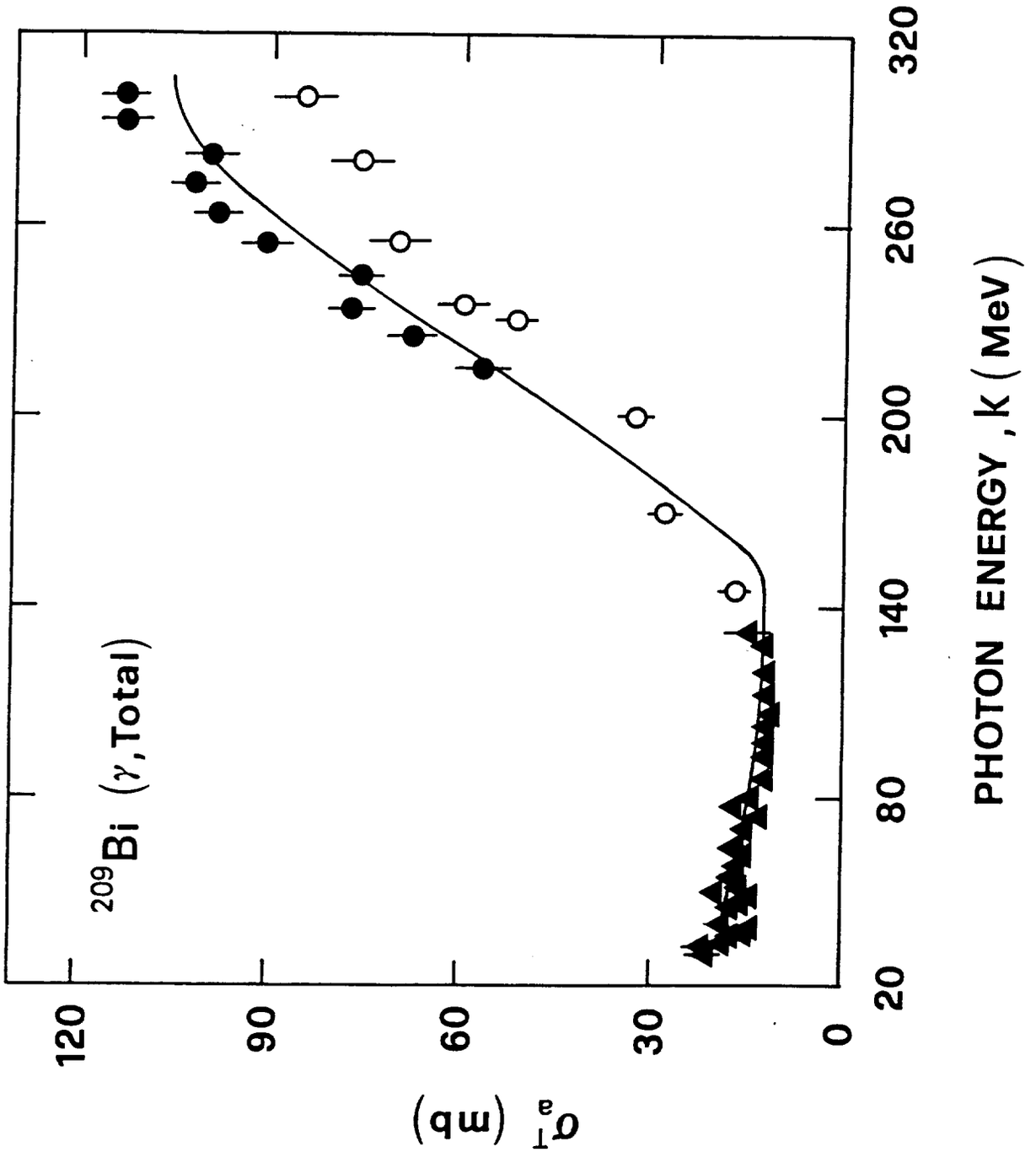
^{209}Bi (γ,Total)
σ_a^T (mb)
120
90
60
30
0
20
80
140
200
260
320
PHOTON ENERGY , k (MeV)

Fig. 3

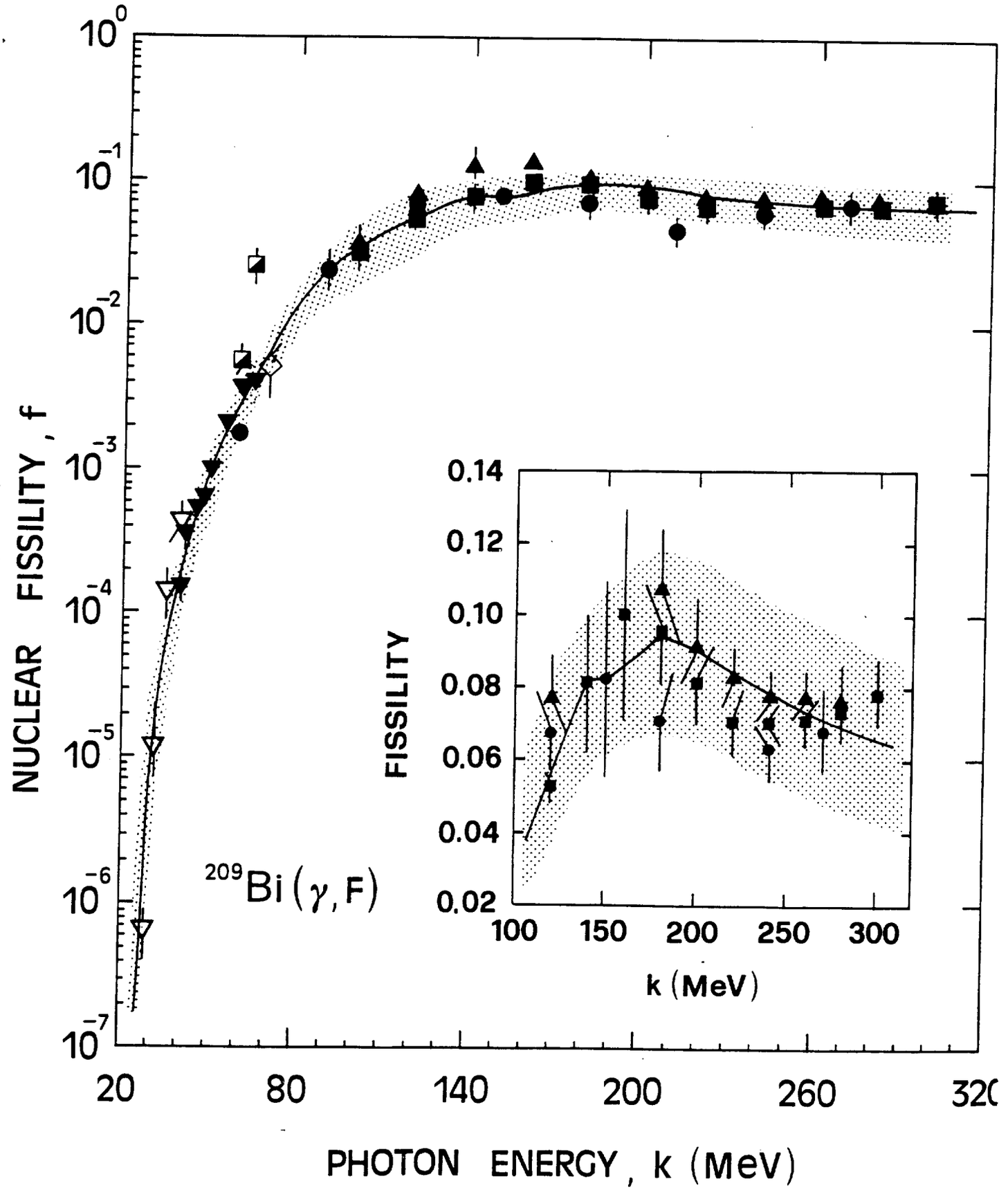
NUCLEAR FISSILITY, f
PHOTON ENERGY, k (MeV)
^{209}Bi (γ, F)
FISSILITY
k (MeV)

Fig. 4

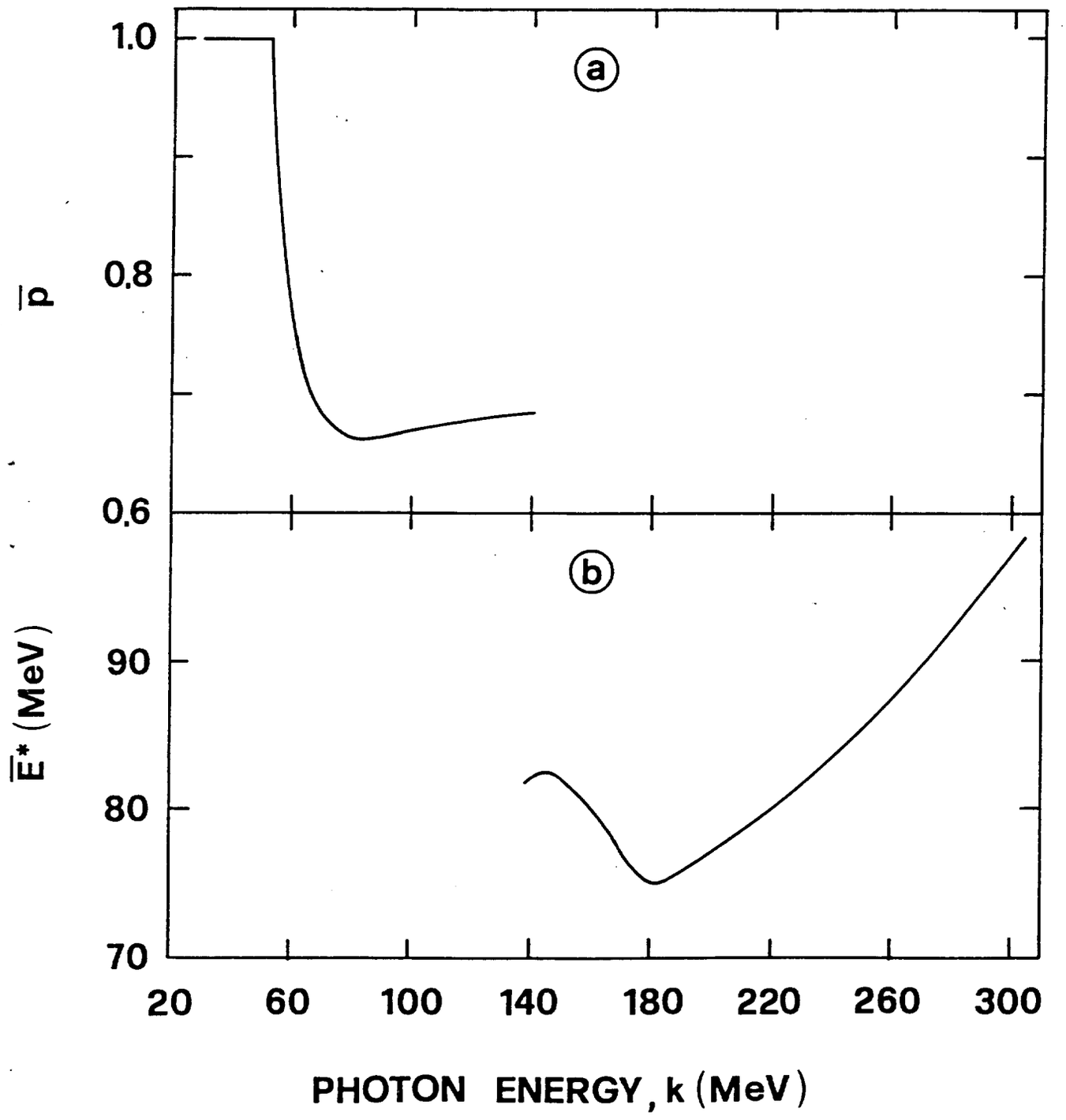
1.0
0.8
0.6
p
a
b
90
80
70
$\bar{E}^*$ (MeV)
20
60
100
140
180
220
260
300
PHOTON ENERGY, k (MeV)

Fig. 5

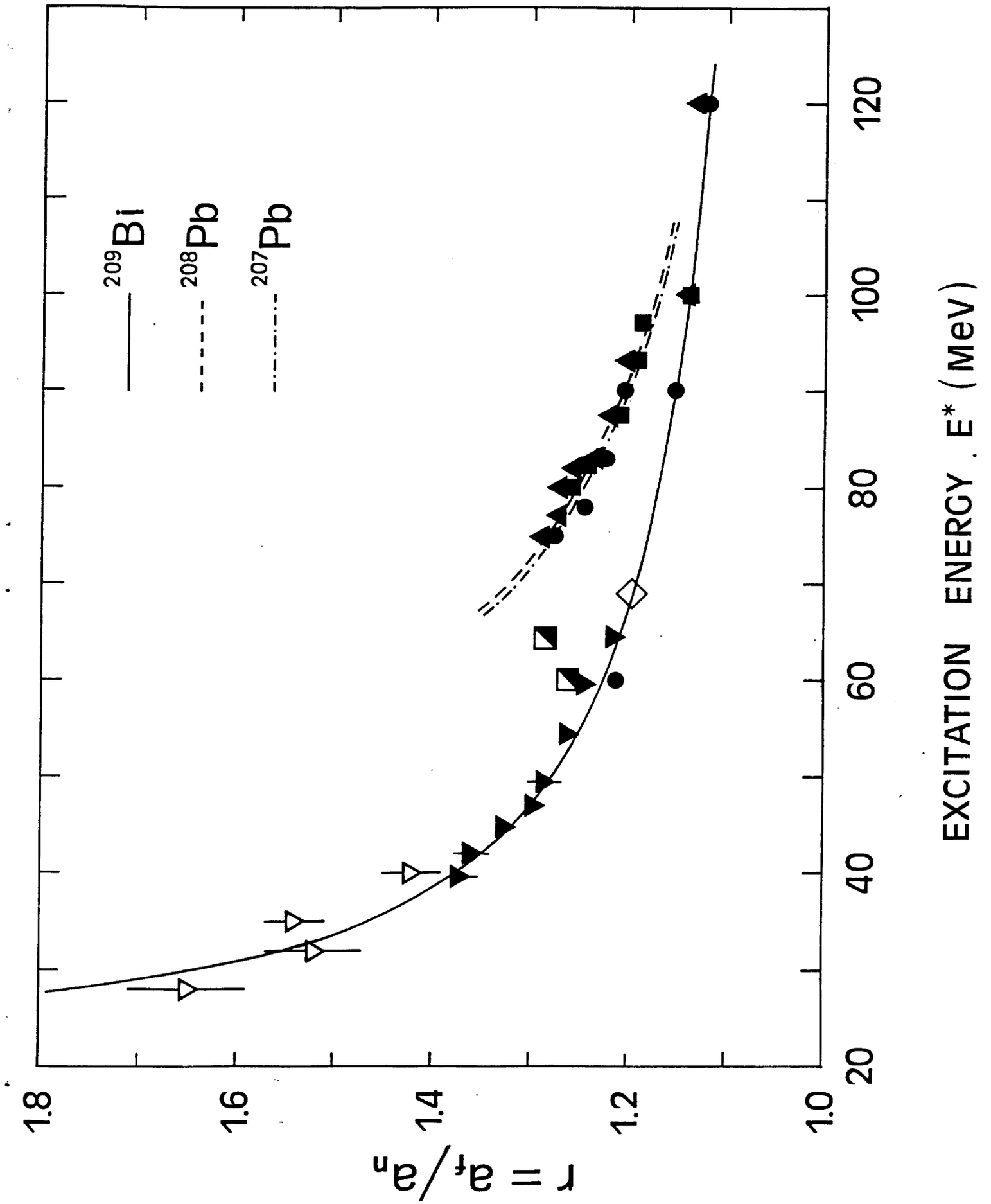
^{209}Bi
^{208}Pb
^{207}Pb
$r = a_f/a_n$
1.8
1.6
1.4
1.2
1.0
20
40
60
80
100
120
EXCITATION ENERGY . E* (MeV)

Fig. 6

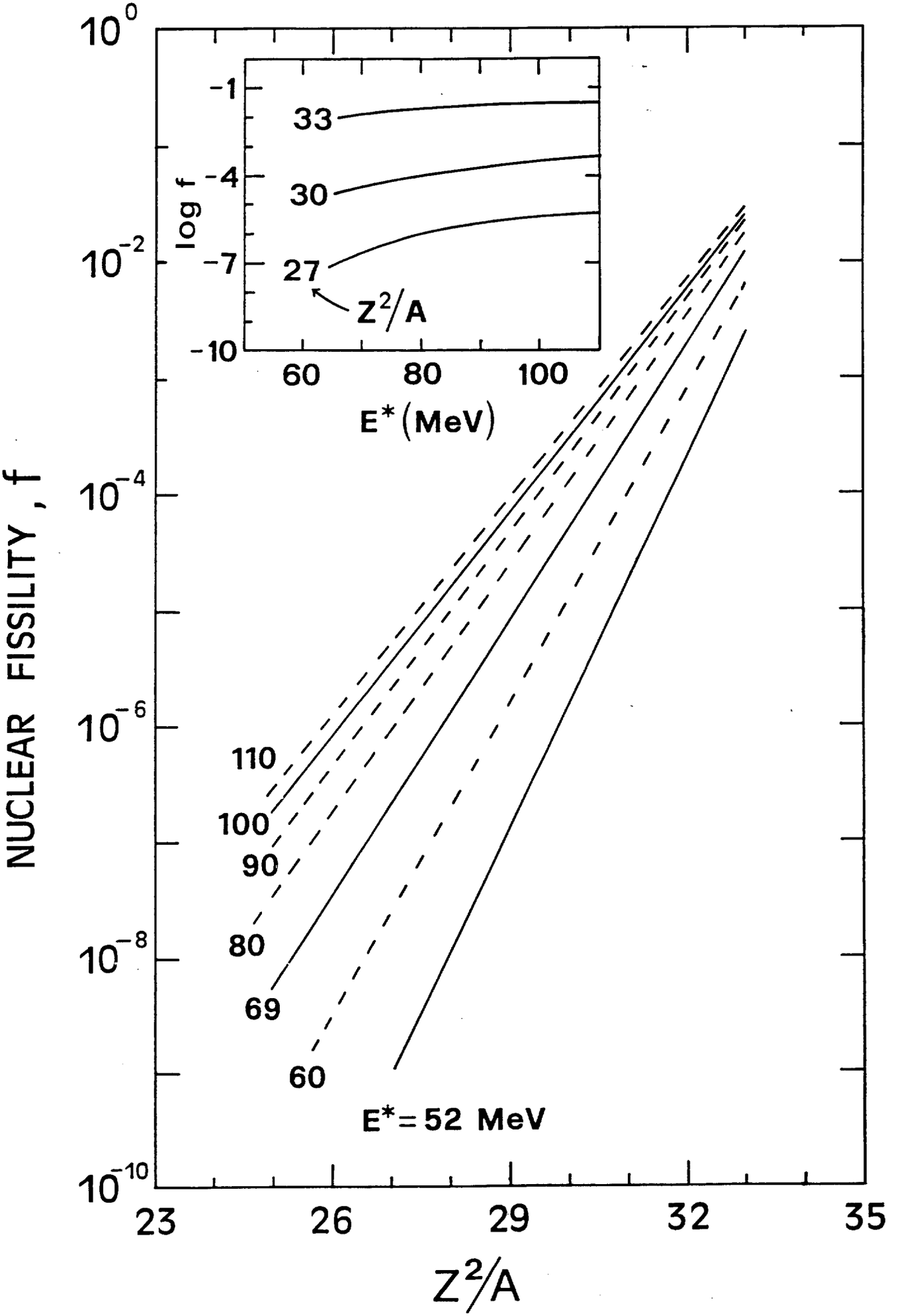
NUCLEAR FISSILITY, f
10^{0}
10^{-2}
10^{-4}
10^{-6}
10^{-8}
10^{-10}
23
26
29
32
35
Z^2/A
110
100
90
80
69
60
E^*=52 MeV
log f
-1
-4
-7
-10
33
30
27
Z^2/A
60
80
100
E^*(MeV)

Fig. 7

TABLE 1 : Values of the ^{209}Bi ground-state fission barrier height , B_{f_0}

Type of determination	Fission barrier B_{f_0} (Mev)	Ref.
Experimental	22.0±1.1	This work[a]
Experimental	21	[2]
Semi-empirical	20.6±2.0	[23]
Experimental	24.3±1.5	[24]
Theoretical	23.9	[25]
Experimental	23.3	[26]
Theoretical	22.4	[27]

[a] Least- squares fitting of photofission cross section data available up to 50 MeV [2,4,20]

Table 2 . The scheme of the two - step model for ^{209}Bi (γ, F) reaction adopted in the present work to calculate nuclear fissility

Energy - range of the incident photon (MeV)	First Step: Photoabsorption mechanism	First Step: Average characteristics of the residual nucleus $\overline{Z}^*$	$\overline{A}^*$	$\overline{E}^*$	First Step: Average probability of formation of the residual nucleus $\overline{p}$	Second Step: De-excitation channels	Second Step: Order of the chance - fission contribution	Calculated Fissility (*)
27 < k < 52	Quasi - deuteron	83	209	k	1	Neutron and fission	only the first	$f = F_1$
52 < k < 80	Quasi - deuteron	83	209	k	Depends on k (fig 5-a)	Neutron and fission	First and second	$f = \bar{p}(F_1 + F_2)$
80 < k <140	Quasi - deuteron	83	209	k	Depends on k (fig 5-a)	Neutron, proton, alpha fission	First and higher order	$f = \frac{2\bar{p}F_1}{1+F_1+G_1+H_1}$
140< k <230	Photomesonic plus Quasi - deuteron	82	208	Depends on k (fig 5-b)	1	Neutron, proton, alpha fission	First and higher order	$f = \frac{2F_1}{1+F_1+G_1+H_1}$
230< k <300	Photomesonic plus Quasi - deuteron	82	207	Depends on k (fig 5-b)	1	Neutron, proton, alpha fission	First and higher order	$f = \frac{2F_1}{1+F_1+G_1+H_1}$

(*) $F_i = \left(\frac{\Gamma_f}{\Gamma_n}\right)_i$, $i = 1, 2$; $G_1 = \left(\frac{\Gamma_p}{\Gamma_n}\right)_1$; $H_1 = \left(\frac{\Gamma_\alpha}{\Gamma_n}\right)_1$. For details see text

CBPF-NF-038/96

REFERENCES

1) Bernardini G , Reitz R, Segre' E 1953 Phys.Rev. 90, 573

2) Warnock R V, Jensen R C 1968 J.inorg. nucl.Chem. 30, 2011

3) de Carvalho H G, Martins J B, Tavares O A P, di Napoli V,Terranova M L, Tesch K 1975 Lett.Nuovo Cimento 14, 615

4) Lemke H D, Ziegler B, Mutterer M, Theobald J P, Cârjan N 1980 Nucl.Phys. A342, 37

5) Bellini V, Emma V, Lo Nigro S, Milone C, Pappalardo G S, De Sanctis E, Di Giacomo P, Guaraldo C, Lucherini V, Polli E, Reolon A R 1983 Lettere Nuovo Cimento 36, 587

6) Guaraldo C, Lucherini V , De Sanctis E, Levi Sandri P, Polli E , Reolon A R, Lo Nigro S, Aiello S, Bellini V, Emma V C , Milone V, Pappalardo G S 1987 Phys.Rev C 36, 1027

7) Martins J B , Moreira E L, Tavares O A P, Vieira J L., Pinheiro Filho J D, Bernabei R, D'Angelo S, De Pascale M P, Schaerf C, Girolami B 1989 Nuovo Cimento 101A, 789

8) Martins J B , Moreira E L ,Tavares O A P , Vieira J L ,Casano L., D'Angelo A, Schaerf C, Terranova M L, Babusci D, Girolami B 1991 Phys.Rev.C 44, 354

9) Kazakov A A, Kezerashvili G Ya,Lazareva L E, Nedorezov V G ,Skrinsky A N, Sudov A S, Tumaikin G M, Shatunov Yu M 1984 Pis'ma Zh.Eksp. Teor. Fiz. 40, 445 [1984 JETP Letters 40 ,1271].

10) Guaraldo C,Lucherini V, De Sanctis E, Iljinov A S, Mebel M V, Lo Nigro S 1990 Nuovo Cimento 103A, 607

11) Kezerashvili G Ya, Muratov V V, Mishnev S I , Ulkraintchev Yu G 1988 *Proceedings of the XI National Conference on Charged Particle Accelerators, Dubna, Russia* vol.1 p.178..

12) Kezerashvili G Ya 1991 *Proceedings of the VIII Int. Conference on Electromagnetic Interactions of Nuclei at Low and Medium Energies, Moscow, Russia* p.16.

13) Kezerashvili G Ya, Milov A M , Wojtsekhowski B B 1991 Preprint Budker Institute of Nuclear Physics (Novosibirsk) B.I.N.P 91-118 p. 13.

14) Kezerashvili G Ya, Milov A M , Wojtsekhowski B B 1993

Nucl.Instr.Meth. A328, 506
15) Tavares O A P 1991 Radiat. Effects Defects Solids 118, 105
16) Iljinov A S , Ivanov D I, Mebel M V, Nedorezov V G, Sudov A S ,Kezerashvili G Ya 1992 Nucl.Phys. A539, 263 ; Ivanov D I , Kezerashvili G Ya, L'vov A I, Mishnev S I, Nedorezov V G, Protopopov I Ya ,Sudov A S 1992 Yad.Fiz. 55 ,3 [1992 Sov.J.Nucl.Phys.55, 1].
17) Alexandrov B M, Ivanov D I, Kezerashvili GYa , Krivokhatsky A S, Muratov V V, Nedorezov V G, Sudov A S, Zapevalov V A 1990 Nucl.Instr.Meth. A288, 399
18) Minarik E V, Novikov V A 1957 J.Exptl.Theoret. Phys. (USSR) 32, 241 [1957 Sov.Phys. JETP 5 ,253].
19) Ranyuk Yu N, Sorokin P V 1967 J.Nucl.Phys. (USSR) 5, 37 [1967 Sov. J.Nucl.Phys. 5 ,26].
20) Moretto L G, Gatti R C, Thompson S G ,Routti J T, Heisenberg J H, Middleman L M ,Yearian M R , Hofstadter R 1969 Phys.Rev. 179, 1176
21) Arruda-Neto J D T ,Sugawara M ,Tamae T, Sasaki O ,Ogino H, Miyase M, Abe K 1985 Phys.Rev. C31, 2321 ; 1986 34, 935
22) Jungerman J A, Steiner H M 1957 Phys.Rev.106, 585
23) Huizenga J R, Chaudhry R, Vandenbosch R 1962 Phys.Rev.126, 210
24) Türck D, Clerc H G , Träger H 1976 Phys.Letters 63B, 283
25) Myers W D, Swiatecki W J 1966 Nucl.Phys.81, 1
26) Moretto L G, Thompson S G, Routti J, Gatti R G 1972 Phys.Lett.38B, 471
27) Myers W D 1977 Droplet Model of Atomic Nuclei , New York, Plenum
28) Levinger J.S 1979 Phys.Lett.B82, 181
29) Tavares O A P, Terranova M L 1992 J.Phys.G: Nucl. Part. Phys. 18 ,521
30) Terranova M L, de Lima D A, Pinheiro Filho J D 1989 Europhys. Lett. 9, 523
31) Rossi P, De Sanctis E, Levi Sandri P, Bianchi N,Guaraldo C,Lucherini V, Muccifora V, Polli E, Reolon A R, Urciuoli G M 1989 Phys.Rev. C 40, 2412
32) Terranova M L, Tavares O A P 1994 Phys.Scripta 49, 267
33) Leprêtre A , Beil H ,Bergère R, Carlos O, Fagot J, De Miniac A,Veyssière A 1981 Nucl.Phys. A367, 237

34) Carlos P, Beil H, Bergère R, Fagot J, Leprêtre A, De Miniac A,Veyssière A 1984 Nucl.Phys. A431, 573
35) Arends J, Eyink J, Hegerath A, Hilger K G, Mecking B, Nöldeke G, Rost H 1981 Phys.Lett. 98B, 423
36) Barashenkov V S, Gereghi F G ,Iljinov A S ,Jonsson G G, Toneev V D 1974 Nucl.Phys. A231 , 462
37) Iljinov A S,Cherepanov E A, Chigrinov S E 1980 Yad.Fiz.32, 322 [1980 Sov.J.Nucl.Phys.32, 166].
38) Leprêtre A, Bergère R, Bourgeois P, Carlos P, Fagot J, Fallou J L, Garganne P ,Veyssière A, Ries H, Göbel R, Kneissl U, Mank G , Ströher H , Wilke W ,Ryckbosch, D, Jury J 1987 Nucl.Phys.A472, 533
39) Lucherini V, Guaraldo C, De Sanctis E, Levi Sandri P ,Polli E, Reolon A R, Iljinov A S , Lo Nigro S, Aiello S, Bellini V, Emma V , Milone C, Pappalardo G S ,Mebel M V 1989 Phys.Rev. C 39, 911 (1989).
40) Iljinov A S, Mebel M V, Guaraldo C, Lucherini V, De Sanctis E, Bianchi N ,Levi Sandri P,Muccifora V, Polli E, Reolon A R ,Rossi P, Lo Nigro S 1989 Phys.Rev. C 39, 1420
41) Tavares O A P, Terranova M L 1992 Z.Phys. A-Hadrons and Nuclei 343, 407
42) Tavares O A P, Terranova M L, Casano, D'Angelo A ,Moricciani D, Schaerf C ,Babusci D ,Girolami B, Martins J B, Moreira E L ,Vieira J L 1991 Phys.Rev. C 44, 1683
43) Levinger J.S 1951 Phys.Rev.84, 43
44) Weisskopf V F 1937 Phys.Rev. 52, 295
45) Vandenbosch R, Huizenga J R 1973 Nuclear Fission , New York , Academic Press (Chapt VII)
46) Fujimoto Y,Yamaguchi Y 1950 Progr.Theor. Phys. 5, 76
47) Iljinov A S, Mebel M V, Bianchi N, De Sanctis E,Guaraldo C,Lucherini V, Muccifora V, Polli E, Reolon A R, Rossi P 1992 Nucl.Phys.A543, 517
48) Arruda-Neto J D T, Saito T, Sugawara M,Tamae T, Miyase H , Abe K , Takahisa K, Konno O, Oikawa M ,Simionatto S 1993 Phys.Rev. C 48, 1594
49) Arruda-Neto J D T,Sugawara M, Miyase H , Kobayashi T, Tamae T, Abe K ,Nomura M, Matsuyama H, Kawahara H, Namai K.,Yoneama M L,Simionatto S 1990 Phys.Rev. C 41, 354

50) Ignatyuk A V, Itkis M G, Okolovich V N, Smirenkin G N ,Tishin A S 1975 Yad.Fiz. 21, 1185 [1975 Sov.J.Nucl.Phys.21, 612].
51) Rostopchin E M, Ostapenko Yu B, Svirin M I,Smirenkin G N 1989 Yad.Fiz. 49, 24 [1989 Sov.J. Nucl.Phys.49, 15].
52) Terranova M L, Tavares O A P, Kezerashvili G Ya, Kiselev V A, Milov A M, Muchnoi N Yu, Naumenkov A I, Petrov V V, Protopopov I Ya, Simonov E A, de Paiva E, Moreira E L 1996 J. Phys. G: Nucl. Part. Phys. 22, 511.

NOTAS DE FÍSICA é uma pré-publicação de trabalho original em Física.
Pedidos de cópias desta publicação devem ser enviados aos autores ou ao:

Centro Brasileiro de Pesquisas Físicas
Área de Publicações
Rua Dr. Xavier Sigaud, 150 – 4º andar
22290-180 – Rio de Janeiro, RJ
Brasil

NOTAS DE FÍSICA is a preprint of original unpublished works in Physics.
Requests for copies of these reports should be addressed to:

Centro Brasileiro de Pesquisas Físicas
Área de Publicações
Rua Dr. Xavier Sigaud, 150 – 4º andar
22290-180 – Rio de Janeiro, RJ
Brazil